Development and application of HVOF sprayed spinel protective coating for SOFC interconnects

Development and Application of HVOF Sprayed Spinel Protective Coating for SOFC Interconnects

O. Thomann, M. Pihlatie, M. Rautanen, O. Himanen, J. Lagerbom, M. Mäkinen, T. Varis, T. Suhonen, and J. Kiviaho

Protective coatings are needed for metallic interconnects used in solid oxide fuel cell (SOFC) stacks to prevent excessive high-temperature oxidation and evaporation of chromium species. These phenomena affect the lifetime of the stacks by increasing the area-specific resistance (ASR) and poisoning of the cathode. Protective $MnCo_2O_4$ and $MnCo_{1.8}Fe_{0.2}O_4$ coatings were applied on ferritic steel interconnect material (Crofer 22 APU) by high velocity oxy fuel spraying. The substrate-coating systems were tested in long-term exposure tests to investigate their high-temperature oxidation behavior. Additionally, the ASRs were measured at 700 °C for 1000 h. Finally, a real coated interconnect was used in a SOFC single-cell stack for 6000 h. Post-mortem analysis was carried out with scanning electron microscopy. The deposited coatings reduced significantly the oxidation of the metal, exhibited low and stable ASR and reduced effectively the migration of chromium.

1. Introduction

Interconnects are required in solid oxide fuel cell (SOFC) stacks to staple together an array of cells in series. Interconnects collect electrons from an anode to the cathode of the neighboring cell, and are the physical barrier between the humid reducing atmosphere on one side and the oxidizing atmosphere on the other. Since SOFCs operate typically at 600-800 °C, the requirement for high-temperature corrosion resistance is high. Additionally, interconnects are designed to ensure homogenous distribution of fuel and oxidant to their respective electrodes. Therefore, their requirements are: (i) high electrical conductivity (i.e., the area-specific resistance (ASR) should be below 100 mΩ cm^2, Ref 1), (ii) high corrosion resistance, (iii) coefficient of thermal expansion (CTE) matching those of the other components of the cell (around 10.5×10^{-6} K^{-1} for yttria-stabilized zirconia electrolyte), (iv) adequate mechanical properties at elevated temperature. At the same time, it is of paramount importance that the material used and the manufacturing

methods are low cost as the high cost of SOFC systems is currently impeding their market entry (Ref 1-3).

Special metallic interconnect alloys such as Crofer 22 APU (ThyssenKrupp VDM), E-Brite (Allegheny Ludlum), or ZMG (Hitachi) are widely used in SOFC stacks as they are cheap compared to ceramic interconnects. State-of-the-art ferritic stainless steel interconnect alloys typically contain 20-25 wt.% Cr to meet the requirements concerning the CTE matching, sufficient oxidation resistance and low cost (Ref 4). At operating conditions, a double oxidation layer is formed consisting of a Cr-oxide layer at the surface of the metal and a Cr-Mn spinel as top layer (Ref 5). These oxide layers prevent the metal from excessive oxidation. However, Cr-oxide growth is associated with an increase in the ASR of the interconnect and is detrimental for the electrical efficiency. The corrosion behavior of the interconnect depends on various factors such as the pre-treatment, alloy composition, operating temperature, gas composition, thickness, and shape. However, it is possible to reduce the corrosion of the interconnect by the application of protective coating (Ref 6).

Another issue with uncoated metallic interconnect is the so-called Cr-poisoning of the cathode. It is by now well established that state-of-the-art SOFC cathodes are poisoned by the volatile Cr-species evaporated from the interconnects and other stainless steel components such as system balance-of-plant components (Ref 5, 7-13). Cr reacts at the cathode current collection to form $SrCrO_4$, increasing the ohmic resistance and additionally Cr-Mn spinel formation can impair the electrochemical activity of the cathode (Ref 12). Alloys specifically designed for interconnect applications exhibit up to 75% reduction of Cr evaporation rate compared to general purpose stainless steels (Ref 5). However, further Cr evaporation rate

O. Thomann, M. Pihlatie, M. Rautanen, O. Himanen, J. Lagerbom, M. Mäkinen, T. Varis, T. Suhonen, and **J. Kiviaho**, VTT Technical Research Centre of Finland, P.O. Box 1000, Espoo 02044 VTT, Finland. Contact e-mail: olivier.thomann@vtt.fi.

reduction is needed to achieve viable stack lifetime for market entry (Ref 14). Therefore, protective coatings are seen as a solution to address the issue of Cr release and the Cr-oxide scale growth of metallic interconnects.

The protective coating requirements are: (i) full density or at least closed porosity, (ii) low diffusivity of Cr and oxygen through the coating, (iii) low ohmic resistance to maximize electrical efficiency, (iv) chemical, physical, and structural compatibility with the adjacent components, e.g., the CTE of the coating and of the substrate must match closely (Ref 1).

A wide variety of protective coatings compositions and manufacturing routes have been reported in the literature and they have recently been the subject of a large review (Ref 6). $(Mn,Co)_3O_4$ spinel coatings have received attention due to their good performance compared to other types of coatings (Ref 15). $(Mn,Co)_3O_4$ spinel coatings have been prepared by slurry spraying (Ref 16, 17), radio-frequency sputtering (Ref 17), magnetron sputtering (Ref 18, 19), plasma spraying (Ref 20), atomic layer deposition (Ref 21), pulsed laser deposition (Ref 22), electrodeposition (Ref 23), and filtered arc (Ref 24). Additionally, $MnCo_{2-x}Fe_xO_4$ has also been tried for its better electrical conductivity (Ref 25, 26). To the authors' knowledge, $(Mn,Co)_3O_4$ and $MnCo_{2-x}Fe_xO_4$ spinel coatings prepared by HVOF spraying for interconnect application have not been previously reported in scientific journals.

Coatings produced on interconnect plates by thermal spraying have been previously reported in the literature. Lim et al. (Ref 27) reported applying $La_{0.8}Sr_{0.2}MnO_3$ (LSM) coating by plasma spraying. The coating was 70-90 μm thick and the ASR was about 20 mΩ cm² at 800 °C after 160 h. Zhai et al. (Ref 28) also reported applying LSM coating on interconnects by plasma spraying. The ASR was measured for 2 h and was ca. 30 mΩ cm². Vargas et al. (Ref 29) reported using atmospheric plasma spraying to produce $MnCo_2O_4$ coating. The coating was ca. 70 μm thick and the ASR was 50 mΩ cm² at 800 °C after 560 h. Cr retention capability was qualitatively evaluated to be sufficient by EDS analysis. Unfortunately, Cr retention is not systematically evaluated in papers reporting protective coatings. It can be evaluated qualitatively by EDS analysis of the coating or quantitatively by the transpiration method (Ref 10, 14, 30). Coatings produced by thermal spraying typically suffer from an as-sprayed lamellar microstructure, and there is a risk of cracking of the coating due to thermal or structural stress (Ref 5, 6). To remedy these issues, optimized powders and spraying parameters can improve the coating quality and ease the risk of fragmentation. In addition to interconnect protective coatings, some stack developers make use of a cathode contact layer of, e.g., $La(Ni,Fe)O_3$ between the protective coating and the cathode of the cell, to establish a good electrical contact (Ref 31).

The development of corrosion-resistant ferritic steels has allowed to use metal plates thinner than 1 mm as interconnect plates. Reducing the thickness of the interconnect allows to use low-cost manufacturing methods such as stamping, cutting, pressing, punching, and hydroforming among others. Additionally, thinner interconnects have a potential for faster start-up by reducing the thermal mass of the stack. But reducing the thickness of the interconnect might increase the corrosion rate because of selective depletion of an alloyed element. A thin plate is more prone to deformation and thus increases the risk of crack formation through the coating.

This article deals with experimental investigations of $MnCo_2O_4$ and $MnCo_{1.8}Fe_{0.2}O_4$ spinel coatings on Crofer 22 APU steel. The aim of the article is to present the results from protective coating development; in the first place the powder manufacturing and optimized coating HVOF method is described. Then, high-temperature oxidation behavior and the ASR of coated steel samples in contact with cathode material are investigated. In order to assess the mechanical behavior of the coating on thin corrugated interconnects, 0.2 mm thin coated corrugated plates were exposed at 700 °C under mechanical load for long-term testing. Furthermore, single-cell stack using the developed coating solution has been run for 6000 h to validate the coating solution in a relevant SOFC environment. The results of the post-mortem analysis of the stack are also presented.

2. Experimental

2.1 Powder Manufacturing

The powders used to produce the spinel coatings were either acquired commercially or manufactured in-house at VTT. The $MnCo_2O_4$ powder was commercial and prepared by the fused and crushed method. $MnCo_{1.8}Fe_{0.2}O_4$ powder was manufactured in-house by solid carbonate synthesis and suitable granule size for thermal spraying was obtained by spray drying. The particle shape of the powder is typically less regular for fused and crushed powders than for spray dried powders. The powder was prepared by weighing appropriate amounts of $MnCO_2$, $CoCO_2$, and Fe_2O_3 powders together and milling for 20 h in a drum ball mill (in-house built). After milling, the mixture was calcined at 1000 °C for 6 h to form the spinel structure. Calcination was done prior to spray drying to avoid granule breakdown due to the large volume change associated to the phase change from the carbonate to oxide. The calcined powder was sieved to below 63 μm. The powder was then ground and dispersed in water with dispersant Dispex A40 by BASF with a Hosokava Alpine AG bead mill (Hydro Mill 90 AHM). The bead milling was continued until average particle size of 1 μm was reached. Polyvinyl alcohol (PVA 22000 by VWR) was used as a bonding agent and was added to the slurry by a dispergator mixer. The PVA addition was carried out just before spray drying to avoid PVA chain shortening during bead milling. The suspension was spray dried with a Niro pilot p6.3 spray dryer. After spray drying parameter optimization, a high rotational speed (20,000 rpm) of centrifugal nozzle was used to obtain fine granule size. The spray dryer includes a cyclone separator and the cyclone fraction was not used further because of its small average particle size and irregular particle shape.

The chamber fraction of the powder was held at 500 °C for 2 h to pyrolyze the PVA without fracturing the agglomerates. Then, sintering occurred at 1150 °C for 6 h. After sintering the powder was sieved with 32 μm sieve. The cyclone fraction was pyrolyzed to remove the PVA and added to the sieved fraction over 32 μm for crushing and recycling to the bead milling stage. The powder fraction below 32 μm was used for HVOF spraying. The powder morphology was studied with Scanning Electron Microscope (SEM, JEOL JSM-636OLV). The crystal structures of the powders and coatings were determined by x-ray diffraction (XRD) using Mo Kα radiation with Philips X'pert diffractometer.

2.2 HVOF Spraying

Commercial Crofer 22 APU steel (ThyssenKrupp) of 0.2 mm thickness was used as substrate material for test coupons. The HVOF coatings were made using a Praxair HV2000 spray gun, fitted with a 22 mm combustion chamber. Nitrogen was used as powder carrier gas (20 slpm), hydrogen as fuel and oxygen as oxidant. For all the reported coatings but one, a hydrogen flow of 700 slpm and an oxygen flow of 350 slpm were used. The $MnCo_2O_4$ coating reported in Fig. 7 was deposited with a hydrogen flow of 687 slpm and an oxygen flow of 315 slpm. The spray gun was moved by an X-Y manipulator. Prior to deposition, the substrates were grit blasted using a −36 mesh alumina grit, brushed and ultrasonically cleaned in acetone. Grit blasting was conducted on both sides to keep the thin metal sheet substrates straight. For the same reason, the coating was applied on both sides. The targeted coating thickness was 20-30 μm, which is unusually thin for thermal spraying. More details on the HVOF coating process can be obtained from Ref 32.

2.3 Exposure Tests

Exposure tests were conducted using laser cut 10 × 10-15 × 0.2 mm samples. The samples were placed standing in a furnace in alumina sample holders so that no contact between samples occurred. The samples were coated on both sides and only the edges of the samples were uncoated. The tests were conducted in air for 1000 h at 700 °C. A continuous gas flow was implemented with the incoming air bubbled through a water bottle; the resulting humidity of the air was thus ~3%. Cross-sectional samples were prepared for SEM observation.

2.4 ASR Measurements

The ASR measurements were done for two coatings ($MnCo_{1.8}Fe_{0.2}O_4$ and $MnCo_2O_4$) applied on two flat 26 × 26 × 0.2 mm steel plates separated by an initially green ceramic layer mimicking a cathode. Additionally, an uncoated steel plate was also tested as a reference. Green 20 × 20 × 1 mm $La_{0.85}Sr_{0.15}Mn_{1.1}O_3$ (LSM) spacers (IRD Fuel Cells A/S, Denmark) were used as separation material between coated steel plates. The purpose of the LSM spacers is to serve as a contact surface with a material similar to a real SOFC cathode. The investigated contact
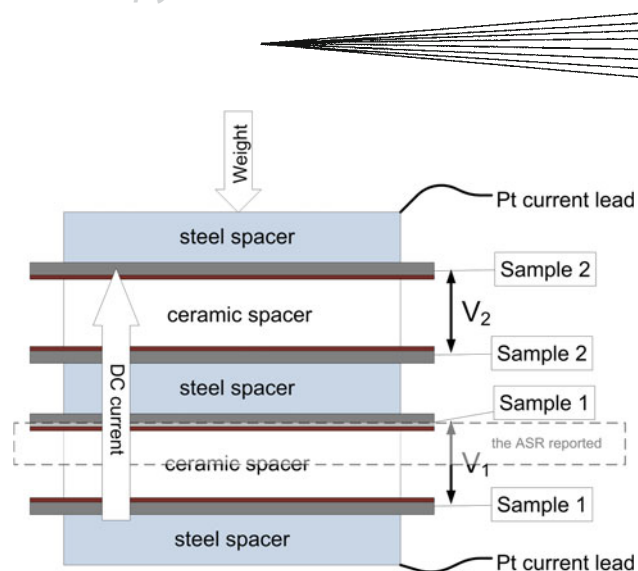

Fig. 1 The ASR measurement arrangement for coated Crofer 22 APU plates with LSM spacers. The protective coatings were applied on the Crofer 22 APU steel surfaces facing the ceramic spacers

resistance interface was therefore coated against LSM. For the experiments, several samples were stacked up and held together by a vertical load of 20 N. A sketch of the test arrangement is shown in Fig. 1. All samples were connected in a single DC current loop, the current was 0.8 A and the current density was 0.2 A/cm². Pt leads of 1 mm were mechanically attached to 1 mm thick steel plates at the bottom and top of the test sample stack. The voltage across each tested material couple was measured by thin (0.3-0.5 mm) Pt threads. To separate each tested substrate-coating system, 1 mm thick steel plates were used as separator disks. The binder was burned out from the green LSM spacers during a slow heat-up at 15 °C/min with a constant flow of air at 0.3 slpm, then the spacers were sintered at the beginning of the experiment for 12 h at 850 °C in contact with the coated steel to form the interface. The steady-state measurements were conducted in compressed filtered dry air at 700 °C during 1000 h. The data were logged using Agilent data logger and multiplexer. The post-mortem analysis was done using JEOL JSM-6335F field emission SEM equipped with a back-scattered electron (BSE) detector and an Oxford Link Pentafet EDS analysator.

2.5 Mechanical Behavior of the Coating in Corrugated Geometry

The coated corrugated samples were tested to examine the effect of mechanical loading and substrate deformation on the HVOF coatings. The corrugated plates were supplied by ECN/ETE (Petten, The Netherlands) and were made by stamping 34 × 4.3 mm corrugations of approximately 1 mm depth into a 0.2 mm plate of Crofer 22 APU (corrugated area: 34 × 34 mm). The HVOF coatings were applied on the corrugated plate and the flat steel plate surfaces and the coatings were placed facing each other.

The mechanical loading was applied by a vertical load of 50 N, causing compressive and tensile stresses at different
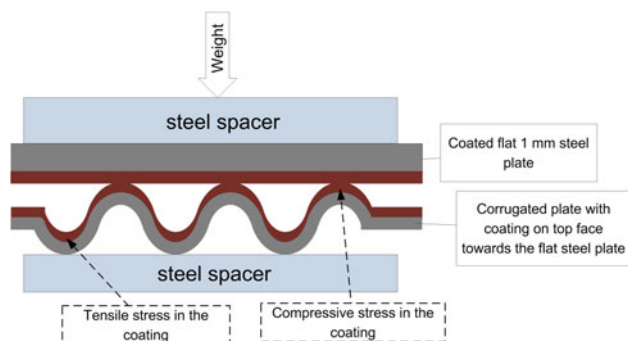
Fig. 2 The arrangement used to investigate the mechanical behavior of the coating on corrugated plates

locations of the coatings as illustrated in Fig. 2. Stationary ambient air was used in the large volume chamber furnace (lid breathable) which secured the sufficient amount of oxygen.

2.6 Stack Testing and Post-mortem Analysis

The $MnCo_{1.8}Fe_{0.2}O_4$ coating was tested in a single-cell stack that was operated for 6000 h at 700 °C. The metallic interconnects were made of 1 mm Crofer 22 APU plates and the gas channels were etched into the plates. Protective coating ($MnCo_{1.8}Fe_{0.2}O_4$) was sprayed on the cathode interconnect with approximately 20 μm as-sprayed thickness. The coated interconnect was not heat-treated and no contact coating was used. Compressible Thermiculite 866 made by Flexitallic Ltd (Cleckheaton, UK) was used as gasket (Ref 33). An anode-supported cell with a (La,Sr)(Co,Fe)O₃ (LSCF) cathode was used. Dry H_2 and dry air were used as fuel and oxidant, respectively. Current density was 0.3 A/cm².

The goals of the post-mortem analysis were to evaluate the coating, the oxide layers present on the cathode interconnect and possible Cr presence in the cathode. After testing, the single-cell stack was mounted in epoxy and cross sections were extracted from the middle area of the cell footprint. Post-mortem analysis was carried out using SEM observation and energy-dispersive x-ray spectroscopy (EDS) on JSM-6400 Scanning Microscope from JEOL equipped with a Prism 2000 detector and Spirit 1.06.02 Analyzer software from Princeton Gamma-Tech (PGT).

3. Results and Discussion

3.1 Powder and Coating Manufacturing

The applied synthesis route using carbonates was found practical in this case because of the simplicity of grinding and therefore thorough mixing of the raw materials. Additionally, the reactivity of the carbonates during calcination was found adequate. If larger amounts of powder would be done industrially, other means of mixing and perhaps other raw materials should be considered to avoid
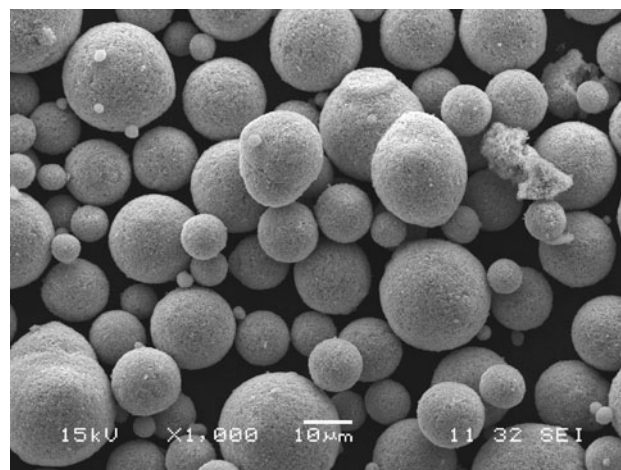

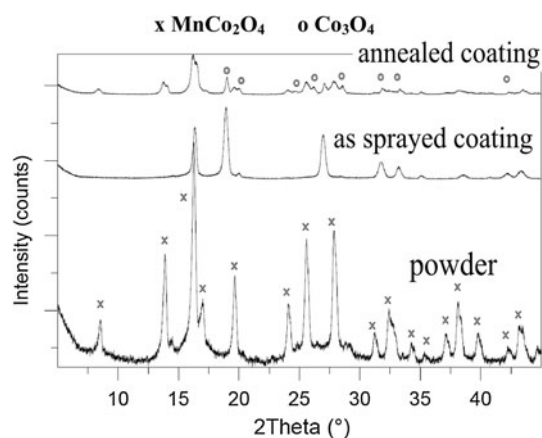**Fig. 3** Secondary electron SEM picture of spray dried $MnCo_{1.8}Fe_{0.2}O_4$ powder

Fig. 4 XRD curves of $MnCo_{1.8}Fe_{0.2}O_4$ powder, coating in as-sprayed state and coating annealed for 2 h at 850 °C. All peaks in the as-sprayed coating correspond to simple cubic phase. The unmarked peaks in annealed coating correspond to the spinel phase $Mn_{1.5}Co_{1.5}O_4$ and $MnCo_2O_4$

the ball milling stage. For instance, chemical synthesis route using dissolved raw materials would ensure homogeneity of the end product.

The $MnCo_{1.8}Fe_{0.2}O_4$ powder prepared by spray drying had typical spherical particle shape which ensures good and constant powder feed rate during spraying. SEM pictures of the powders are presented in the Fig. 3. Only small amount of fine satellites can be seen on larger particles surface. This amount was not considered to cause any problems for HVOF spraying; dusting and feed issues were minimal. Using regular shape powder increases the deposition efficiency and decreases the amount of defects in the coating.

Illustrated in Fig. 4, the XRD pattern of $MnCo_{1.8}Fe_{0.2}O_4$ powder sintered at 1150 °C corresponds to the $MnCo_2O_4$ spinel structure. The XRD pattern of the coating in its as-sprayed state shows that the phase structure is changed during the coating process to simple cubic

structure corresponding for example to the structure of CoO and MnO (space group *Fm*-3*m*). This structure is a metastable state formed because of rapid cooling of the spray droplets during thermal spraying. The XRD curve of the coating after 2 h of annealing at 850 °C shows that the coating crystal structure transforms mainly to the spinel structures $Mn_{1.5}Co_{1.5}O_4$, Co_3O_4, and $MnCo_2O_4$. Exposure for longer time to the actual SOFC environment will fully transform the crystal structure to $MnCo_2O_4$ (Ref 32).

3.2 Exposure Tests

Figure 5 shows a typical microstructure of a $MnCo_2O_4$ as-sprayed protective coating made by HVOF; the coating shows typical lamellar structure and adequate density. Some alumina particles can be observed in the steel-coating interface from the grit blasting procedure. Oxidized steel with a HVOF $MnCo_{1.8}Fe_{0.2}O_4$ coating of 15-18 μm thickness is shown in Fig. 6 after exposure to air for 1000 h at 700 °C; the microstructure is shown in Fig. 6(a) and (b) and elemental profile from an EDS line scan is shown in Fig. 6(c). The Cr oxide layer formed between the steel and the coating during the exposure is about 0.5 μm. During high-temperature exposure, the coating sinters and loses its lamellar structure. Some closed porosity remains visible still after 1000 h of exposure with a decreasing porosity toward the surface. There is little or no Cr gradient in the coating (Fig. 6c), which means that the diffusion of Cr is effectively hindered. As a reference on oxidation, a non-coated Crofer 22 APU sample exposed to the same oxidizing conditions showed in microscopy an oxide layer of 2.5-3 μm of thickness, which is five times higher than for the coated sample. Therefore, the coating solution effectively reduces the oxidation of the steel interconnect.
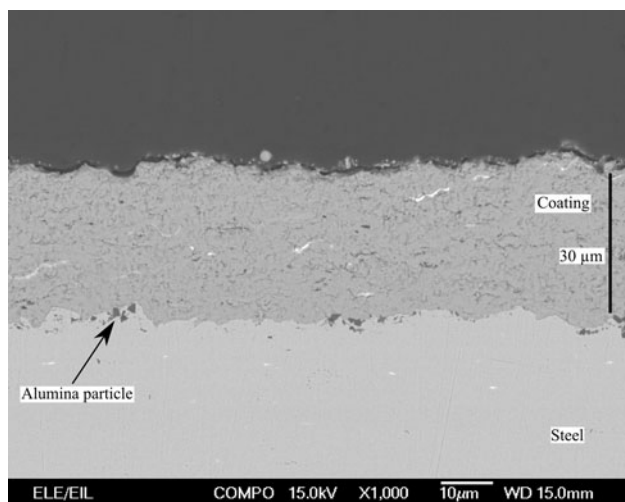
3.3 ASR Measurements

The ASR measurements against time for coated and uncoated Crofer 22 APU steel are illustrated in Fig. 7. The reported ASR represents half of the ASR measured for one repeating unit in the sample stack shown in Fig. 1. The different components contributing to the ASR value consist of the steel substrate, the Cr oxide scale developing on the steel substrate surface, the protective coating, the contact resistance of the interface between the coating and the ceramic cathode material and the resistance of the ceramic cathode material (i.e., the resistance of 500 μm of LSM cathode material). The reason for the step change in the ASR taking place at 220 h is not completely understood, but is probably related to a structural instability. The change taking place at 720 h of the test in the $MnCo_{1.8}Fe_{0.2}O_4$ sample which was tested in a second test run is due to a small unintentional change in the test temperature (10 °C) due to a power shutdown. For the three samples, the test temperature was between 690 and 710 °C during the long-term test.

The ASRs of the $MnCo_{1.8}Fe_{0.2}O_4$ (15-18 μm thick) and the $MnCo_2O_4$ (20-28 μm thick) coatings are initially 20-30 mΩ cm^2 and decrease slightly to about 20 mΩ cm^2 during the first few hundred hours and then remain stable over the tested period. These results show that the coating solution is adequate to prevent degradation of the electric properties of the interconnect during SOFC operation. Comparisons of ASR values between different studies are delicate because the experimental parameters such as ASR measurement temperature, aging time, and type of spacer used are inconsistent throughout the literature. However, these ASR results are in line with results reported for similar types of coatings (Ref 6) or using a similar test arrangement (Ref 17, 34). The improvements of the ASRs during the first few hundred hours of test are attributed to the sintering of the initially lamellar coating.

The ASR of the bare Crofer 22 APU in contact with LSM is initially about 100 mΩ cm^2 and decreases throughout the tested period to reach 45 mΩ cm^2 after 1000 h of test. The observed decrease of ASR over time is mainly due to improvement in the electrical contact between steel and LSM. Both coatings show initially much lower ASRs compared to the bare Crofer 22 APU. The main source of the difference between the bare Crofer 22 APU and the coated samples is believed to originate from a lower contact resistance of the coated samples.

3.4 Mechanical Behavior of the Coating on Corrugated Geometry

The effect of the corrugated geometry on the mechanical behavior of HVOF $MnCo_2O_4$ coatings was investigated with SEM by looking at different locations of the corrugated geometry. The coating at the top of the corrugation ridges experiences a compressive force when the mechanical loading is applied. The load tends to straighten the corrugation by causing permanent plastic deformation (creep). Consequently, the coating at the bottom of the corrugation groove experiences a tensile
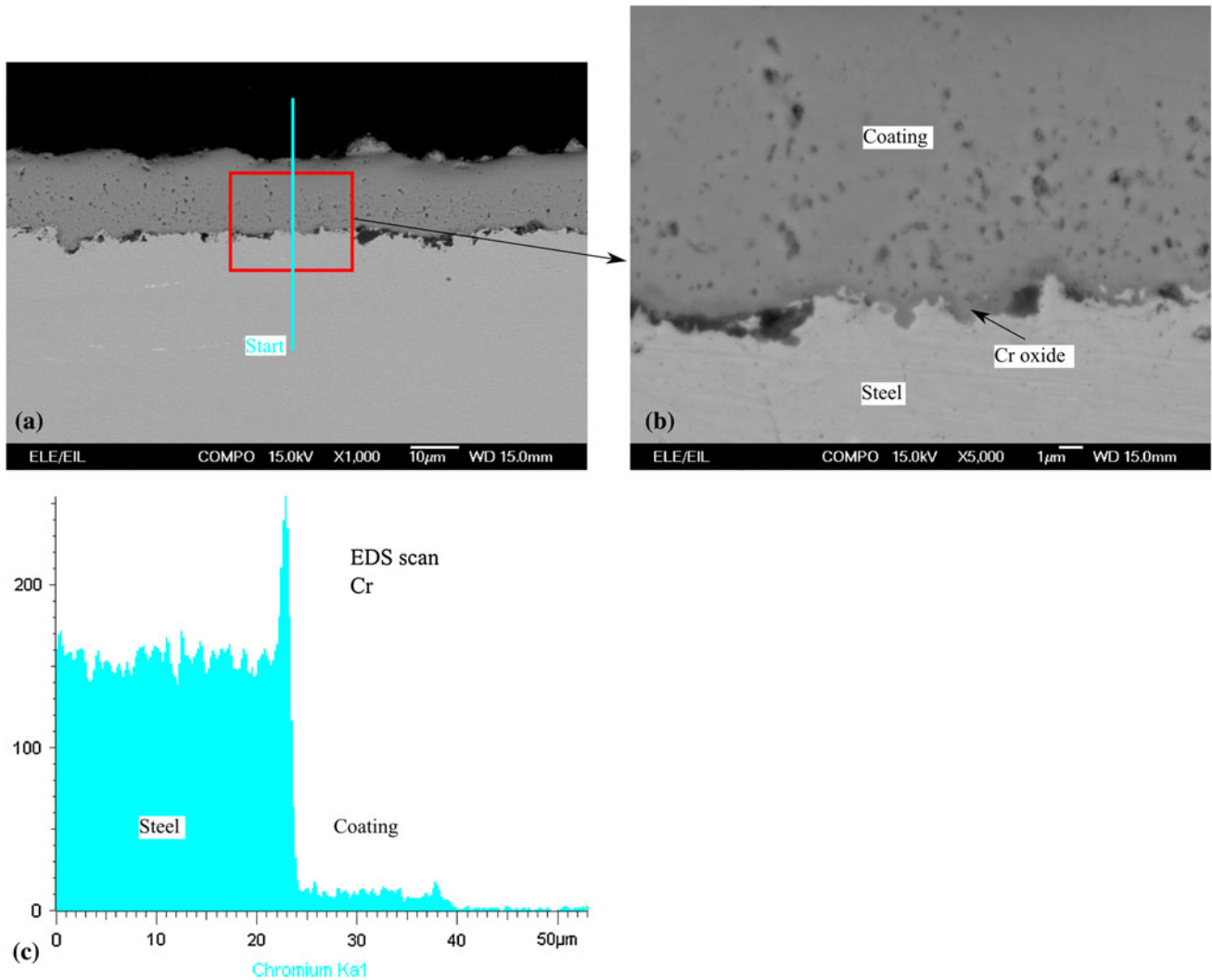

Fig. 5 A BSE SEM image of an as-sprayed HVOF $MnCo_2O_4$ coating on Crofer 22 APU substrate

Fig. 6 (a) and (b) BSE SEM images of a HVOF $MnCo_{1.8}Fe_{0.2}O_4$ coating on Crofer 22 APU substrate exposed to air at 700 °C for 1000 h at different magnifications. (c) Measured Cr EDS profile
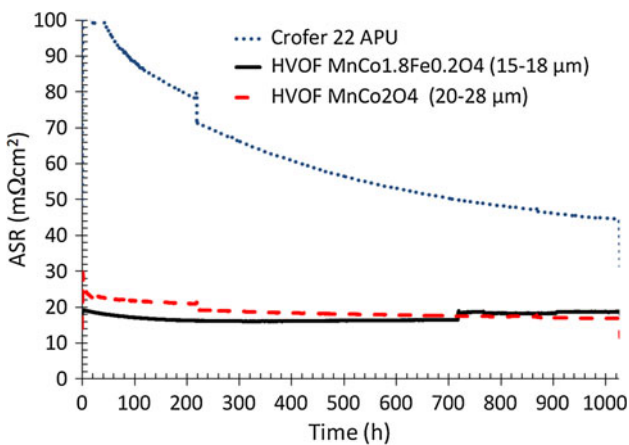

Fig. 7 Measured ASR in a 4-point DC measurement of Crofer 22 APU, coated and uncoated, all in contact with a LSM spacer. The coatings are $MnCo_{1.8}Fe_{0.2}O_4$ and $MnCo_2O_4$

stress. After a 1000 h exposure test at 700 °C, the HVOF coating at the top of the corrugation was largely intact as depicted in the SEM micrograph in Fig. 8(a). Conversely, several through-coating cracks were observed at the bottom of the groove due to tensile stress combined with the intrinsic brittleness of $MnCo_2O_4$ material and coating structure, Fig. 8(b). The stress needed for the fracture of the coating will depend closely on the distribution of flaws in the scale as well as the stress field, but it seems evident that the stresses had in this case been relaxed by through-coating cracks in the HVOF coating. Therefore, while the basic protective function of the HVOF coatings are well fulfilled, they may not be optimal for stack designs having metallic interconnects made of thin corrugated steel plates because of their propensity for cracking under tensile stress due to mechanical load. Although the steel interface at the bottom of the cracks do not show any accelerated corrosion in the present case, such effects or Cr release through the cracks could possibly take place in long-term operation. However, crack formations could possibly be
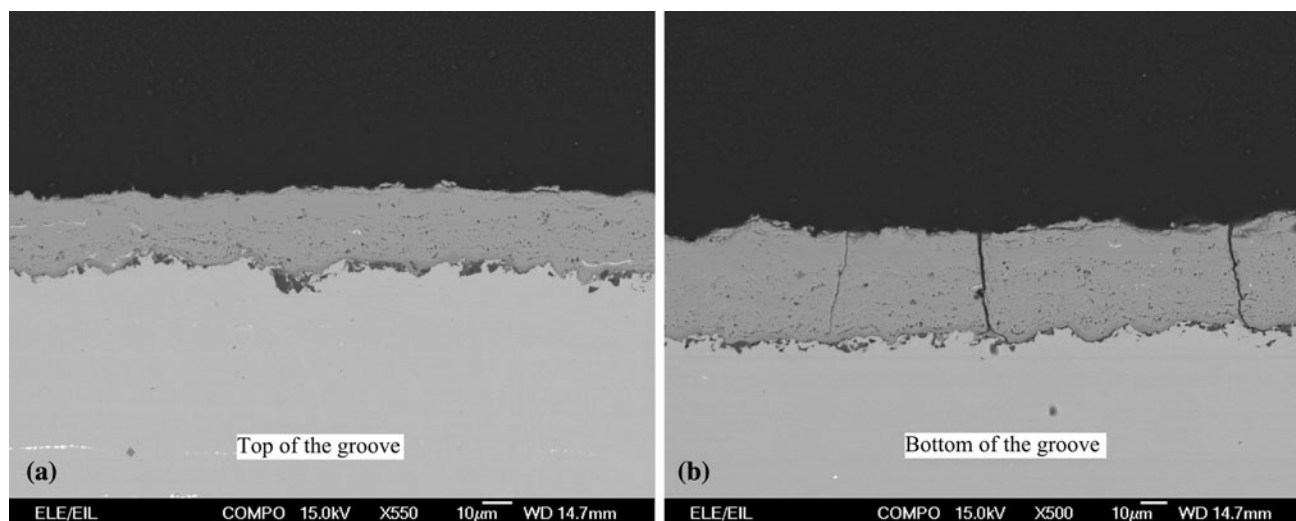
Fig. 8 SEM images from the top (a) and bottom (b) of the corrugated profile exposed to a vertical mechanical load in a high-temperature exposure test with a HVOF MnCo$_2$O$_4$ coating (1000 h at 700 °C in air)

avoided by adjusting the design of the corrugation and thickness of the interconnect.

3.5 Single-Cell Stack Post-mortem Analysis

Four BSE SEM images of the single-cell stack are presented in Fig. 9. Figure 9(a) shows a low-magnification view of the cathode side of the single-cell stack where the air channel and the contact location between the interconnect and the cathode are visible. It is clear that the coating covers the interconnect completely, including the geometrically challenging features such as the edges of the interconnect ribs. The gap between the cathode and electrolyte and the cracks found in the coating at the air channels are due to sample preparation.

Figure 9(b) shows the contact location between the cathode side of the cell and the coated interconnect with MnCo$_{1.8}$Fe$_{0.2}$O$_4$. The micrograph shows good contact between cathode and interconnect. The Cr-oxide scale at the surface of the interconnect metal is about 1 μm in thickness after 6000 h at 700 °C in air. This result can be compared to the exposure tests presented in section 3.2 where the Cr-oxide layer of coated steel was about 0.5 μm thick and the Cr-oxide layer of the unprotected steel was about 2.5-3 μm after 1000 h in air at 700 °C. Therefore, it can be concluded that the coating acts as an effective protection and reduces oxidation of the interconnect in a long-term test in SOFC environment. No cracks are visible in the coating itself, however closed porosity is still present. EDS analysis was performed on the area shown in Fig. 9(b) and no Cr was found neither in the coating nor in the cathode which indicates that Cr diffusion and evaporation through the coating is effectively hindered.

Figure 9(c) shows another micrograph of the coating at an air channel location. The coating presents no cracks but some closed porosity similarly to Fig. 9(b). The Cr-oxide layer under the coating is also about 1 μm thick and no Cr could be detected in the coating. Figure 9(d) illustrates the cathode located at an air channel and a EDS Cr concentration profile. As already mentioned, there is a large gap between cathode and the electrolyte (out of the picture) due to sample preparation and therefore the cathode stands alone in the epoxy. An EDS analysis of the cathode reveals that Cr was present in the cathode at this air channel location. Cr distribution is inhomogeneous and peaks at 2.1 at.%. However, most of the Cr is located away from the active cathode area which is located close to the electrolyte; therefore, the deposited Cr has probably not affected the electrochemical performance of the cathode. The Cr contamination can be either coming from the stainless steel interconnect through the protective coating or from the uncoated Crofer 22 APU air manifold and Inconel 600 air inlet pipe upstream of the cell. However, Cr deposit was located at the air channel (corresponding to Fig. 9d) and not at the contact location with the interconnect (corresponding to Fig. 9b), which supports the hypothesis that Cr has originated from the uncoated air manifold and inlet pipe. Additionally, from the EDS analysis performed across the coating, negligible Cr diffusion appears to take place across the coating. Stainless steel components and manifold upstream of the cells have been previously identified as Cr contamination sources in SOFC stacks (Ref 10, 35). From these results, the coating solution is adequate for steel interconnect protection as it reduces effectively both Cr evaporation and steel interconnect oxidation.

4. Conclusions

Protective MnCo$_2$O$_4$ and MnCo$_{1.8}$Fe$_{0.2}$O$_4$ coatings were manufactured on SOFC steel interconnects by HVOF coating. Exposure tests showed that a 1000 h oxidation in air at 700 °C resulted in a Cr oxide layer of 0.5 μm for the steel protected by HVOF coating. In
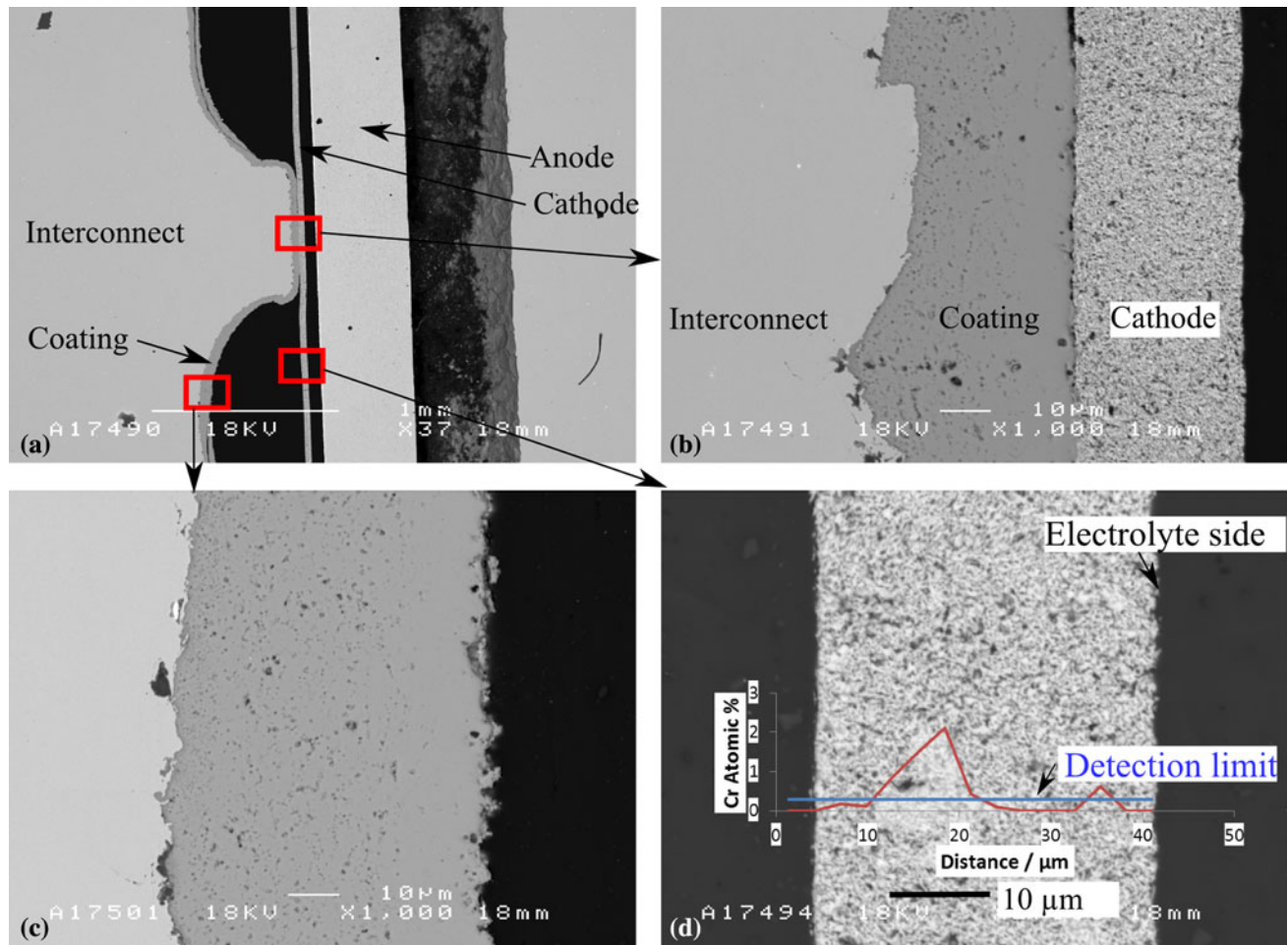
Fig. 9 BSE SEM cross section from the single-cell stack at different locations. (a) Low-magnification image of the air side of the single-cell stack. The interconnect coating composition is $MnCo_{1.8}Fe_{0.2}O_4$. (b) Contact area between coated interconnect and cathode. (c) Surface of the interconnect at an air channel location. (d) Cathode with an EDS Cr profile

comparison, uncoated steel sample developed a 2.5-3 μm Cr oxide layer in the same conditions.

ASR measurements were carried out at 700 °C for 1000 h on coated steel samples in contact with LSM spacers. The results confirmed low ASR values for coated samples of about 20-30 mΩ cm^2 with no degradation over time. These results show that the HVOF coating method developed at VTT is a suitable candidate to be used in SOFC stacks. The mechanical behavior of the coating was evaluated by applying a mechanical load on a coated corrugated thin plate. It was found that the stress arising from deformation of the plate leads to crack formation where the coating is under tension. Therefore, if such corrugated geometry is used for interconnect, more crack-resistant coating solution should be developed.

The protective coating showed adequate corrosion protection and retention of Cr in a single-cell stack test up to 6000 operation hours. The Cr oxide layer was about 1 μm thick and the coating was crack-free and Cr-free. A low concentration of Cr was detected in the fuel cell cathode; however, the uncoated steel manifold and piping upstream of 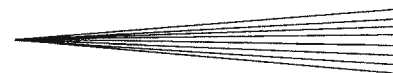the stack test setup are known to be a source of volatile Cr and are likely to be the origin of the Cr found in the cathode.

Acknowledgments

References

1. J. Wu and X. Liu, Recent Development of SOFC Metallic Interconnect, *J. Mater. Sci. Technol.*, 2010, **26**(4), p 293-305
2. J.W. Fergus, Metallic Interconnects for Solid Oxide Fuel Cells, *Mater. Sci. Eng. A*, 2005, **397**(1–2), p 271-283

3. W.Z. Zhu and S.C. Deevi, Development of Interconnect Materials for Solid Oxide Fuel Cells, *Mater. Sci. Eng. A*, 2003, **348**(1–2), p 227-243

4. Z. Yang, K.S. Weil, D.M. Paxton, and J.W. Stevenson, Selection and Evaluation of Heat-Resistant Alloys for SOFC Interconnect Applications, *J. Electrochem. Soc.*, 2003, **150**(9), p A1188-A1201

5. M. Stanislowski, E. Wessel, K. Hilpert, T. Markus, and L. Singheiser, Chromium Vaporization from High-Temperature Alloys, *J. Electrochem. Soc.*, 2007, **154**(4), p A295-A306

6. N. Shaigan, W. Qu, D.G. Ivey, and W. Chen, A Review of Recent Progress in Coatings, Surface Modifications and Alloy Developments for Solid Oxide Fuel Cell Ferritic Stainless Steel Interconnects, *J. Power Sources*, 2010, **195**(6), p 1529-1542

7. H. Tu and U. Stimming, Advances, Aging Mechanisms and Lifetime in Solid-Oxide Fuel Cells, *J. Power Sources*, 2004, **127**(1–2), p 284-293

8. M.C. Tucker, H. Kurokawa, C.P. Jacobson, L.C. De Jonghe, and S.J. Visco, A Fundamental Study of Chromium Deposition on Solid Oxide Fuel Cell Cathode Materials, *J. Power Sources*, 2006, **160**(1), p 130-138

9. J.A. Schuler, H. Yokokawa, C.F. Calderone, Q. Jeangros, Z. Wuillemin, A. Hessler-Wyser, and J. Van Herle, Combined Cr and S Poisoning in Solid Oxide Fuel Cell Cathodes, *J. Power Sources*, 2012, **201**, p 112-120

10. O. Thomann, M. Pihlatie, J.A. Schuler, O. Himanen, and J. Kiviaho, Method for Measuring Chromium Evaporation from SOFC Balance-of-Plant Components, *Electrochem. Solid-State Lett.*, 2012, **15**(3), p B35-B37

11. J.W. Fergus, Effect of Cathode and Electrolyte Transport Properties on Chromium Poisoning in Solid Oxide Fuel Cells, *Int. J. Hydrogen Energy*, 2007, **32**(16), p 3664-3671

12. N.H. Menzler, P. Batfalsky, L. Blum, M. Bram, S.M. Groß, V.A.C. Haanappel, J. Malzbender, V. Shemet, R.W. Steinbrech, and I. Vinke, Studies of Material Interaction After Long-Term Stack Operation, *Fuel Cells*, 2007, **7**(5), p 356-363

13. K. Hilpert, D. Das, M. Miller, D.H. Peck, and R. Weiß, Chromium Vapor Species Over Solid Oxide Fuel Cell Interconnect Materials and their Potential for Degradation Processes, *J. Electrochem. Soc.*, 1996, **143**(11), p 3642-3647

14. M. Stanislowski, J. Froitzheim, L. Niewolak, W.J. Quadakkers, K. Hilpert, T. Markus, and L. Singheiser, Reduction of Chromium Vaporization from SOFC Interconnectors by Highly Effective Coatings, *J. Power Sources*, 2007, **164**(2), p 578-589

15. Y. Larring and T. Norby, Spinel and Perovskite Functional Layers Between Plansee Metallic Interconnect (Cr-5 Wt% Fe-1 Wt% Y_2O_3) and Ceramic (La0.85Sr0.15)0.91MnO$_3$ Cathode Materials for Solid Oxide Fuel Cells, *J. Electrochem. Soc.*, 2000, **147**(9), p 3251-3256

16. X. Chen, P.Y. Hou, C.P. Jacobson, S.J. Visco, and L.C. De Jonghe, Protective Coating on Stainless Steel Interconnect for SOFCs: Oxidation Kinetics and Electrical Properties, *Solid State Ion.*, 2005, **176**(5–6), p 425-433

17. Z. Yang, G. Xia, G.D. Maupin, and J.W. Stevenson, Conductive Protection Layers on Oxidation Resistant Alloys for SOFC Interconnect Applications, *Surf. Coat. Technol.*, 2006, **201**(7), p 4476-4483

18. Y. Fang, C. Wu, X. Duan, S. Wang, and Y. Chen, High-Temperature Oxidation Process Analysis of $MnCo_2O_4$ Coating on Fe-21Cr Alloy, *Int. J. Hydrogen Energy*, 2011, **36**(9), p 5611-5616

19. A. Balland, P. Gannon, M. Deibert, S. Chevalier, G. Caboche, and S. Fontana, Investigation of La_2O_3 and/or $(Co, Mn)_3O_4$ Deposits on Crofer22APU for the SOFC Interconnect Application, *Surf. Coat. Technol.*, 2009, **203**(20–21), p 3291-3296

20. J. Puranen, J. Lagerbom, L. Hyvärinen, T. Mäntylä, E. Levänen, M. Kylmälahti, and P. Vuoristo, Formation and Structure of Plasma Sprayed Manganese-Cobalt Spinel Coatings on Preheated Metallic Interconnector Plates, *Surf. Coat. Technol.*, 2010, **205**(4), p 1029-1033

21. K. Uusi-Esko, E. Rautama, M. Laitinen, T. Sajavaara, and M. Karppinen, Control of Oxygen Nonstoichiometry and Magnetic Property of $MnCo_2O_4$ Thin Films Grown by Atomic Layer Deposition, *Chem. Mater.*, 2010, **22**(23), p 6297-6300

22. L. Mikkelsen, M. Chen, P.V. Hendriksen, Å. Persson, N. Pryds, and K. Rodrigo, Deposition of La0.8Sr0.2Cr0.97V0.03O$_3$ and $MnCr_2O_4$ Thin Films on Ferritic Alloy for Solid Oxide Fuel Cell Application, *Surf. Coat. Technol.*, 2007, **202**(4–7), p 1262-1266

23. M.J. Lewis and J.H. Zhu, A Process to Synthesize (Mn, Co)$_3$O$_4$ Spinel Coatings for Protecting SOFC Interconnect Alloys, *Electrochem. Solid-State Lett.*, 2011, **14**(1), p B9-B12

24. V.I. Gorokhovsky, P.E. Gannon, M.C. Deibert, R.J. Smith, A. Kayani, M. Kopczyk, D. Vanvorous, Z. Yang, J.W. Stevenson, S. Visco, C. Jacobson, H. Kurokawa, and S.W. Sofie, Deposition and Evaluation of Protective PVD Coatings on Ferritic Stainless Steel SOFC Interconnects, *J. Electrochem. Soc.*, 2006, **153**(10), p A1886-A1893

25. X. Montero, N. Jordán, J. Pirón-Abellán, F. Tietz, D. Stöver, M. Cassir, and I. Villarreal, Spinel and Perovskite Protection Layers between crofer22APU and La 0.8Sr0.2FeO$_3$ Cathode Materials for SOFC Interconnects, *J. Electrochem. Soc.*, 2009, **156**(1), p B188-B196

26. J. Puranen, J. Lagerbom, L. Hyvärinen, M. Kylmälahti, O. Himanen, M. Pihlatie, J. Kiviaho, and P. Vuoristo, The Structure and Properties of Plasma Sprayed Iron Oxide Doped Manganese Cobalt Oxide Spinel Coatings for SOFC Metallic Interconnectors, *J. Therm. Spray Technol.*, 2011, **20**(1–2), p 154-159

27. D.P. Lim, D.S. Lim, J.S. Oh, and I.W. Lyo, Influence of Post-Treatments on the Contact Resistance of Plasma-Sprayed La 0.8Sr 0.2MnO$_3$ Coating on SOFC Metallic Interconnector, *Surf. Coat. Technol.*, 2005, **200**(5–6), p 1248-1251

28. H. Zhai, W. Guan, Z. Li, C. Xu, and W.G. Wang, Research on Performance of LSM Coating on Interconnect Materials for SOFCs, *J. Korean Ceram. Soc.*, 2008, **45**(12), p 777-781

29. M.J. Garcia-Vargas, M. Zahid, F. Tietz, and A. Aslanides, Use of SOFC Metallic Interconnect Coated with Spinel Protective Layers Using the APS Technology, *ECS Trans.*, 2007, **7**, p 2399

30. M. Casteel, P. Willson, T. Goren, P. O'Brien, and D. Lewis, Novel Method for Measuring Chromia Evaporation from SOFC Interconnect Materials, *ECS Trans.*, 2009, **2**(5), p 1411

31. R.N. Basu, F. Tietz, O. Teller, E. Wessel, H.P. Buchkremer, and D. Stöver, LaNi0.6Fe0.4O$_3$ as a Cathode Contact Material for Solid Oxide Fuel Cells, *J. Solid State Electrochem.*, 2003, **7**(7), p 416-420

32. J. Lagerbom, T. Varis, J. Puranen, M. Pihlatie, O. Himanen, V. Saarinen, J. Kiviaho, and E. Turunen, $MnCo_2O_4$ Spinel Chromium Barrier Coatings for SOFC Interconnect by HVOF, *9th Liège Conference on Materials for Advanced Power Engineering*, 2010, p 925–932

33. J.R. Hoyes and S. Bond, Gaskets for Sealing Solid Oxide Fuel Cells, *Seal. Technol.*, 2007, **8**, p 11-14

34. L. Mikkelsen, K. Neufeld, and P.V. Hendriksen, Interface Resistance Between FeCr Interconnects and La0.85Sr0.15Mn1,1O$_3$, *ECS Trans.*, 2009, **25**, p 1429

35. J.A. Schuler, Z. Wuillemin, A. Hessler-Wyser, C. Comminges, N.Y. Steiner, and J. Van Herle, Cr-Poisoning in (La, Sr)(Co, Fe)O$_3$ Cathodes After 10,000 h SOFC Stack Testing, *J. Power Sources*, 2012, **211**, p 177-183